Materials & Design 260 (2025) 115212

Contents lists available at ScienceDirect

Materials & Design

journal homepage: www.elsevier.com/locate/matdes

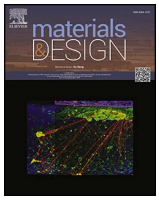

Development of novel castellated functionally graded W/EUROFER coatings for fusion application

Ashwini Kumar Mishra *, Thilo Grammes, Jarir Aktaa

Karlsruhe Institute of Technology (KIT), Institute for Applied Materials, Hermann-von-Helmholtz-Platz 1, 76344 Eggenstein-Leopoldshafen, Germany

ARTICLE INFO

Keywords:
Tungsten coatings
Castellation
Thermal fatigue test
Plasma spraying
Finite element simulations
Plasma-facing components

ABSTRACT

W/EUROFER functionally graded material (FGM) coatings have application in the First Wall of fusion plants as a shielding layer. In this work, a novel castellation of W/EUROFER coatings has been developed. Castellation is defined as cuts or notches created in material to reduce the thermal stress. Finite element simulations of castellated coatings were performed to evaluate the advantage of the castellation. Simulations suggested a reduction in the bending of coated components as well as a reduction of residual stress. Afterwards, simulations were performed to find out the optimized depth of castellation. Simulations of castellated and non-castellated coated sections under a heat flux cycle showed a reduction in bending of the coated section with castellation as compared to the non-castellated coating section. Castellation experiments were executed on coated samples using the optimized depth. After castellation, recovery in the original coating-induced deflection of the samples indicated the feasibility of the castellation approach. Additionally, thermal fatigue tests were performed on castellated coated samples to determine the thermal load stability of the notch. Neither cracks at the notch tip nor the interface are observed for at least 5000 cycles of thermal load typical for the envisaged fusion application.

1. Introduction

Tungsten has high sputtering resistance, high thermal conductivity, high melting point, and low neutron activation properties [1,2], which make it a suitable candidate for a protection layer in the First Wall of future fusion plants. EUROFER97 steel has been selected as a structural material in the DEMOnstration Power Plant First Wall, with a tungsten (W) coating as a shielding over it. Some recently developed tungsten coating methods include plasma spraying, chemical vapor deposition (CVD), laser cladding, field assisted sintering technique (FAST), cold spray, and physical vapor deposition (PVD) [3–10]. Apart from coatings, tungsten fiber-reinforced tungsten [11] was also developed as a plasma-facing material.

However, high thermal stresses will be induced between W and steel due to the difference in the thermal expansion coefficient of W and EUROFER steel. Thermal stresses can be developed during the coating deposition and operation of the fusion plant, which will be the limiting factor of the lifetime of these plasma-facing components. These thermal stresses can be reduced by a functionally graded W/EUROFER interlayer between the W top coating and steel. Weber et al. [12] demonstrated a reduction in thermal stress due to a gradient interlayer during thermal cycles using the finite element method. Vaßen et al. [4] showed a gradient in residual stress across the gradient coating thickness after deposition, measured by the incremental hole drilling method. W/EUROFER FGM coatings have already been achieved on the laboratory scale and the industrial scale [4–6,13–16]. An additional way to reduce thermal stress in plasma-facing components is castellation. Castellation has been used for plasma-facing components for various materials as reported in the literature [7,17–23].

Li et al. [19] have discussed about the castellation of W coating by spraying a vacuum plasma spray (VPS) coating (W/Cu gradient interlayer and pure W) over a castellated CuCrZr heat sink. They analyzed the reduction of thermal stress by castellation. However, the optimized study of castellation in coatings was not performed. Xu et al. [20] have experimentally examined the castellation in the W/oxygen-free Cu (OFC)/CuCrZr mock-up in which the notch was machined in the top W layer. They observed cracks near the notched end in the W tile during a high heat flux test. The maximum stress accumulated in the region was reported as a cause of these cracks by simulations. Bobin Vastra et al. [21] have performed a thermal fatigue test on a W coating with a

* Corresponding author.
E-mail address: ashwini.mishra@kit.edu (A.K. Mishra).

https://doi.org/10.1016/j.matdes.2025.115212
Received 6 May 2025; Received in revised form 17 October 2025; Accepted 24 November 2025
Available online 24 November 2025

castellation and a uniform W surface. In both cases, the number of sustained cycles was found to be the same. Sharafat et al. [22] have developed a micro-engineered textured tungsten coating that acts as a micro-castellation of coating using chemical vapor deposition (CVD). Cui et al. [7] have deposited W coatings with vertical cracking which acts similar to castellation. However, in the case of vertical crack coating, the depth of the crack and position cannot be precisely controlled. Zammuto et al. [23] have found cracks close to the tip of the notch in castellated ASDEX Upgrade (AUG) W tiles. They also reported the possibility of micro-cracks at the tip of the notch during the manufacturing process.

Although the W/EUROFER functionally graded coating has reduced the residual stress, the remaining residual stress is still responsible for the bending of larger coated components (half-meter scale), as observed in [6]. Castellation can reduce the residual stress developed during deposition and hence the bending of coated components. This is of particular importance when considering the size of future First Wall elements in DEMO (scale of multiple meters) [24].

Based on the available literature, the castellation of W/EUROFER coating has not been explored. The problems with the existing castellation of W tiles call for an optimization study. The objective of this work is to propose an optimized castellation of W/EUROFER FGM coatings. Initially, the finite element method is used to study the reduction in residual stress and bending of steel by castellation. Afterward, simulations are performed with various notch depths to determine the optimized notch depth without any plastic deformation in the steel. Then, a thermo-mechanical simulation was performed with and without castellation coating under the DEMO First Wall relevant heat flux cycle conditions to compare performance. Subsequently, experimental castellation of the coated component is performed to check the reduction in bending of the coated component which indicates the relief of residual stress developed during deposition. This validates qualitatively the hypothesis that castellation relieves residual stresses in the coating and reduces the bending of coated steel. This is followed by a thermal fatigue test of W/EUROFER FGM coating samples with optimized notch depth to analyse the effect of the notch under thermal stress.

2. Simulation and experimental procedures

2.1. Finite element modelling

Two-dimensional (2-D) finite element simulations were performed using ABAQUS CAE 2022. A small, coated section (22 mm × 5 mm) was simulated here, as shown in Fig. 1. The 2-D model consists of a 0.8 mm W top layer, then 1.2 mm of functionally graded W/EUROFER coating, and finally 20 mm of EUROFER steel substrate. Functionally graded W/EUROFER coating consists of 5 interlayers, each of equal thickness (240 μm) and varying W contents from 25, 37, 50, 63, and 75 vol% from interlayer-1 (IL-1) to interlayer-5 (IL-5).

XY directions are shown in Fig. 1a. The boundary conditions of the small, coated section in FEM were provided such that it becomes equivalent to a small section of a large, coated plate. The lower left node is restricted from moving in the y-direction to provide stability in the model. An x-symmetry boundary condition was applied to the left side of the model, as shown in Fig. 1a. The edge effect doesn't exist in a small section of a large, coated component. Hence, a kinematic coupling constraint was applied to the right side of the model to prevent edge effects in the FEM model and simulate stress conditions for a small section in a larger coated section. By this constraint, the right side can move (translate and rotate) with its nodes remaining on a straight line. Generalized plane strain elements (CPEG-4) are suitable to simulate the behaviour of plates using a representative 2D section of it. The elastic-ideal plastic material properties and thermal expansion coefficient properties of W [12,25] and EUROFER [12,26,27] were used in the simulations from the literature. Properties of the interlayer were taken by the rule of mixture using the fraction of W and EUROFER in each

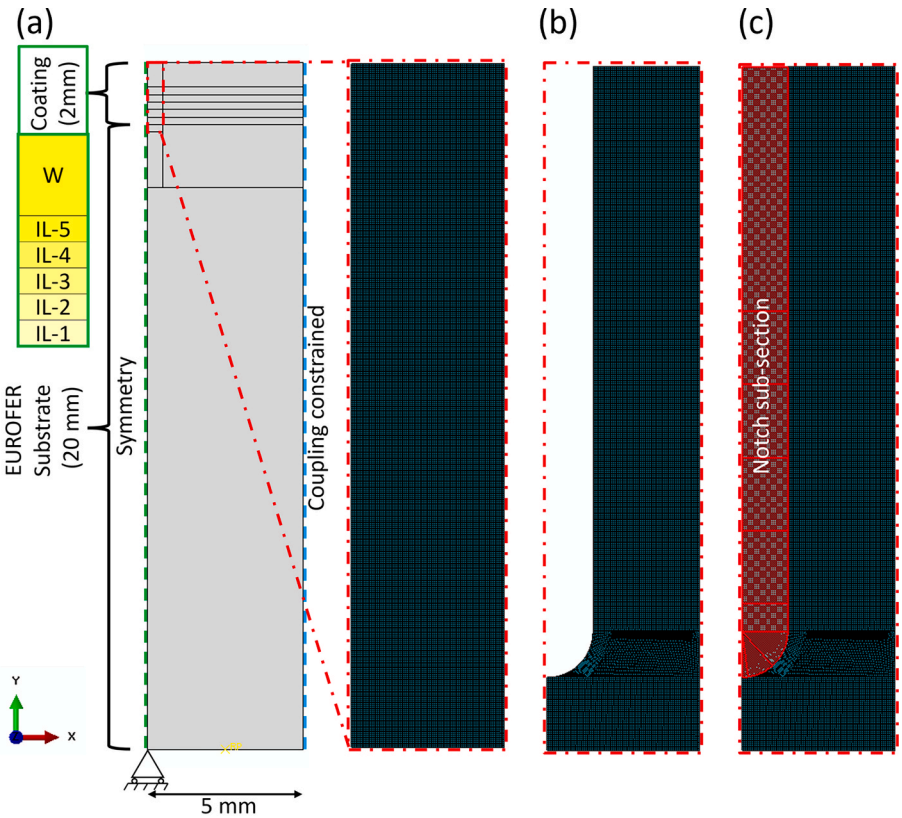

Fig. 1. FEM model of a coated section a) without notch showing details of boundary condition and mesh b) with a notch during deposition c) with a sub-section of a notch for simulating a notch machined after deposition.

interlayer. The rule of mixture was used to determine the gradient coating interlayer properties for FEM simulation, as suggested in the references [28–30].

Three sets of simulations were performed as shown in Fig. 1. The first case simulation was performed without any notch for the comparison. The whole model was homogeneously cooled from a stress-free state at 750 °C to 20 °C to obtain the residual stresses developed during coating. Simulations were performed to determine the residual stress during the cooldown process, without considering possible temperature variation during the deposition. A similar way of simulation was used in the literature [13,30] to determine the residual stresses in the coating. In the second case simulation, a notch was introduced in the model as shown in Fig. 1b. The simulations were performed by cooling the whole model from a stress-free state at 750 °C to 20 °C to get the residual stresses similar to the coating condition. In the third case, a sub-section was defined as a notch as shown in Fig. 1c. For the third simulation, the whole model was first cooled from a stress-free state at 750 °C to 20 °C to get the residual stresses similar to the first case. Then, in the next step, the notch sub-section was deactivated, allowing stress relaxation. The third model was to represent the condition when the notch was machined after the coating. At the same time, the second model represents the notch during the deposition. In both cases, the notch depth was 2 mm and its width 0.3 mm. In the FEM model, the notch width is 0.15 mm because of the symmetry boundary condition. A small sub-section was created on the left side of the model, to create a refined mesh at the notch root. The third case of simulation was repeated with varying notch depth to determine the optimized notch depth suitable for castellation.

Afterward, a steady state thermo-mechanical finite element simulation was performed for the first case and the third case (optimized notch depth) under a heat flux cycle. The purpose of this simulation was to compare the effect of castellation during a heat flux cycle resembling the DEMO First Wall conditions. Generalized plane strain thermally coupled (CPEG4T) mesh elements were used for the simulation. In addition to elastic-ideal plastic material properties and thermal expansion coefficient properties, a thermal conductivity of W [31] and EUROFER [27] was used in the model. Boundary conditions were the same as previous simulations, as shown in Fig. 1a.

Simulation of the first case (without a notch) was performed in three steps. In the first step, the whole model of the first case was cooled from 750 °C to 20 °C to simulate the residual stresses, similar to deposition conditions. Then in the second step, the whole model was heated to 300 °C. In the third step, a surface heat flux cycle was applied on the top surface of the coating, while the bottom surface of the steel was maintained at 300 °C (coolant temperature in the DEMO First Wall). The heat flux cycle consists of a heating phase (10 s) and a cooling phase (10 s). Three different maximum heat fluxes of 0.25, 0.34, and 0.35 MW/m^2 were applied as a thermal load to determine the maximum temperature in the FEM model. The heat flux cycle, which generates a maximum temperature of less than 550 °C, was chosen as a representative of the heat flux cycle in the DEMO first wall. The planned maximum temperature for DEMO First Wall is 550 °C. Chelihi et al. [32] have recently demonstrated a thermo-mechanical simulation of DEMO First Wall using a heat flux of 0.25 MW/m^2. In our case, the simulation was performed at three different values to determine the maximum temperature. The difference is due to the absence of a cooling channel in our FEM model.

Similarly, simulation of the third case (optimized notch depth) under a heat flux cycle was performed in four steps. The first step was similar to the previous case, cooling the whole model from 750 °C to 20 °C. In the second step, the notch sub-section was deactivated, allowing stress relaxation while maintaining the model temperature at 20 °C. Then the third and fourth steps were heating the whole model to 300 °C and applying a surface heat flux cycle on the top surface of the coating while maintaining the bottom surface of the steel at 300 °C, respectively. This model represents the condition in which the notch was machined after the coating process and then subjected to a heat flux.

2.2. Experimental procedure

W/EUROFER functionally graded coatings were deposited using a low-pressure plasma spraying method on a P92 steel substrate of dimensions 50 × 50 × 20 mm^3 and 500 × 250 × 20 mm^3 (with cooling channels) by the company COATEC GmbH (Schlüchtern, Germany). Deposition details were given in reference [6]. Although EUROFER will be used in the DEMO First Wall, P92 was instead used due to its higher availability and similar properties [27,33–35].

Five large samples/strips of the dimensions 224 × 20 × 22 mm^3 were machined using electric discharge machining from the large coated plate (500 mm × 250 mm) for the initial experiments of castellation. These large samples were prepared to measure the recovery in deflection due to castellation notches, which indicates the relief of residual stresses. Fig. 2a shows one of these samples before the castellation. The thickness of the W coating and FGM layer was 790 μm ± 26 μm (standard deviation, S.D) and 1196 μm ± 67 μm (S.D), respectively. The desired notch depth in 3 samples (S_L1 to S_L3) was 1388 μm ± 43 μm (S.D), nearly half of the FGM layer. While in 2 samples (S_L4 and S_L5), an optimized notch depth of 1627 μm ± 54 μm (S.D) was machined. Accordingly, the notch depth of S_L3 was further increased to 1627 μm ± 54 μm. The optimized notch depth was based on the FEM results (section 3.1.2). These notches were machined between the cooling channels at a distance of 13 mm from each other. In total 16 notches were machined in every sample. The deflection of the samples was measured using a 3D coordinate measuring machine (Crysta-PlusM 574, Mitutoyo, Neuss, Germany). These measurements were performed at the center of the bottom side of the samples before and after machining notch.

Fig. 2b shows the SEM image of the deposited coating from a 50 mm × 50 mm coated plate. The thickness of the top W coating and functionally graded layer were 874 μm ± 24 μm (S.D) and 1283 μm ± 10 μm (S.D) respectively. 6 cylindrical samples of length 20 mm and 5 mm diameter were prepared using electric discharge machining from the coated 50 mm × 50 mm steel plate. 5 cylindrical samples are shown in Fig. 2c. A desired notch of depth 1772 μm ± 25 μm (S.D) was machined in the samples. The desired notch depth was chosen as the sum of the thickness of the W layer and 70 % of the FGM layer and was decided based on the FEM results as will be explained in section 3.1.2. The actual notch depth of all samples was measured and given in Table 1. The actual notch depth was found very close to the desired one.

Thermal fatigue tests were performed using a customized testing setup described in the reference [36]. Fig. 3a shows the image of the thermal fatigue test chamber, which shows the sample and induction coil.

The thermal fatigue test setup was made of a cylindrical stainless steel chamber with 2 induction coils (maximum 1.5 kW) for heating the sample which can hold 2 samples. Samples were held inside the induction coils with the help of ceramic holders that are not affected by induction heating. This chamber was closed from the top (ISO sealing) with an inlet for argon gas. Ar gas was used to create an inert atmosphere and allow fast cooling. Two pairs of thermocouples were attached to two samples by spot welding. The temperature was controlled by LabVIEW software. Temperature uniformity within a sample was verified for the test setup in the reference [36]. The difference between the temperature at the coating/substrate interface and the center of the sample was ≤7 °C. During the thermal fatigue test, a maximum of 120 W of induction power (8 % of the maximum output of the induction heat system) was used for heating the sample and 5 l/min of Argon gas was used for cooling. At the start of the test, the chamber was purged by Ar gas about 5 times the volume of the chamber. The initial five cycles of two samples are shown in Fig. 3b. The thermal fatigue test was performed by heating and cooling the samples between 550 °C and 300 °C. These temperatures are the nominal values input in the LabVIEW software. The actual temperatures of the samples were measured by the thermocouples. The

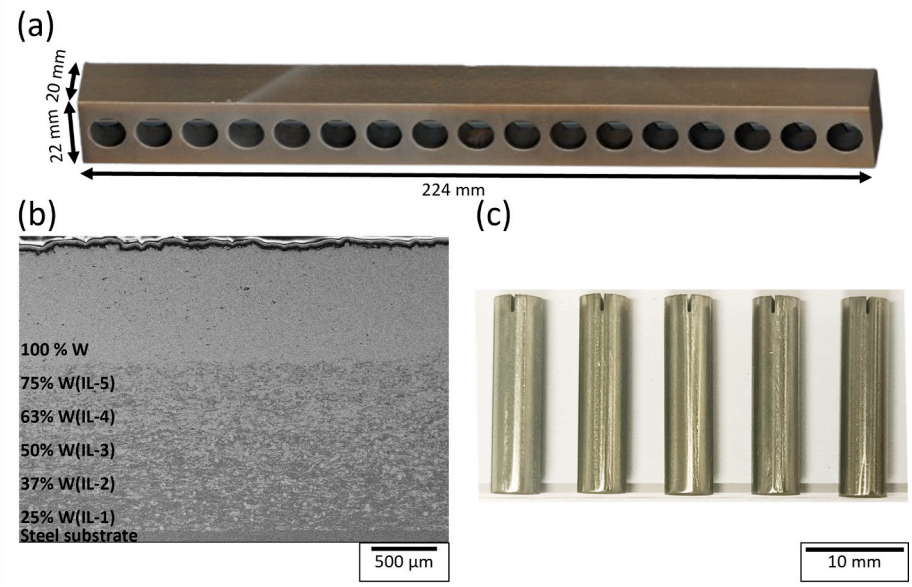

Fig. 2. a) Large coated sample with cooling channels used for castellation experiment b) scanning electron microscopy (SEM) image of a cross-section of W/EUROFER coating and substrate c) cylindrical sample of diameter 5 mm and 20 mm length with notch for thermal fatigue test.

Table 1
Details of notched thermal fatigue samples. The error shows standard deviation.

Sample No.	Notch depth (µm)			No. of cycle	T(min) °C			T(max) °C		
S1	1825	±	12	0						
S2	1805	±	15	500	298	±	1	555	±	3
S3	1801	±	8	1000	270	±	1	551	±	0
S4	1778	±	12	1500	288	±	2	551	±	1
S5	1780	±	6	2000	298	±	1	551	±	1
S6	1788	±	16	5000	295	±	4	564	±	14

average maximum and minimum temperatures of the samples are shown in Table 1. 5 samples were tested with 500, 1000, 1500, 2000, and 5000 cycles. Two samples were tested together such that 1 sample was fixed for 5000 cycles while the other 4 samples were changed after the corresponding number of cycles. Thermal fatigue tests were performed up to 5000 cycles, which is 5 times the number of operation cycles (1000) planned for the DEMOnstration reactor [37].

After the thermal fatigue test, these samples were cut perpendicular to the notch for cross-section imaging. The samples were prepared by the standard metallographic polishing method. Cross-section images of the sample were taken using scanning electron microscopy (SEM, EVO MA10, Zeiss, Oberkochen, Germany).

3. Results and discussion

3.1. Simulation results

3.1.1. Effect of castellation

Fig. 4 shows the residual stress contours (S_{11} stress) for all three simulation conditions. The maximum compressive stress in top W coating was found in the FEM model of the coated section without a notch (Fig. 4a). In the second case of simulation, where a notch was considered during deposition, residual stress relief was observed (Fig. 4b). The residual stresses are developed due to a thermal expansion mismatch between the coating and the steel substrate. The notch allows slight deformation in the coating, relaxing the stresses created during deposition. This yields a decrease in the compressive residual stresses in the top W coating and all the interlayers. The top W layer becomes nearly stress-free near the notch. Also, the tensile residual stress in the substrate near the notch was reduced as compared to without notch deposition.

In the third case, the notch was formed after the coating process which similarly helps in the relief of residual stresses (Fig. 4c). Residual

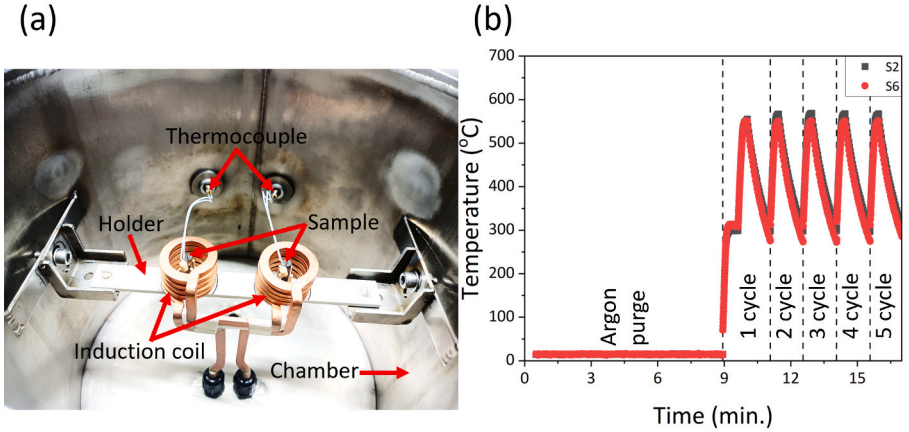

Fig. 3. a) Inside view of the thermal fatigue test chamber b) first 5 cycles of 2 thermal fatigue samples tested.

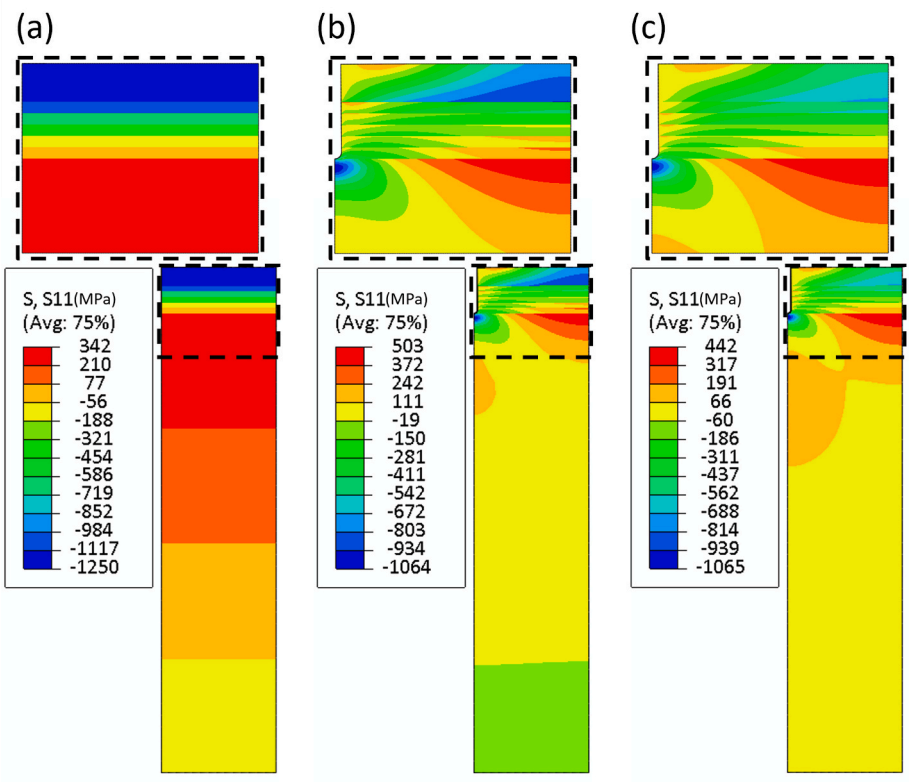

Fig. 4. Residual stresses (S_{11}) contour of a) coated section without notch b) coated section with notch during deposition c) coated section with notch after deposition.

stress relief was expected due to the removal of material. Similar to the second case, in the third case also, the compressive stresses in the top W coating and interlayers were lower than coating without a notch (case-1). Reduction in the tensile stresses in the steel substrate near the notch was also similar to the 2nd case of the simulation. A tensile stress in steel away from the notch was increased for cases 2 and 3 as compared to case 1. The tensile stress in steel was maximum in case 2 and minimum in case 1, while intermediate in case 3. However, the tensile stress in steel was lower than the yield stress in all cases, so no plastic deformation was observed because of that. Therefore, this slight increase in tensile stress should not be a critical problem.

Comparing the 2nd and 3rd cases, the maximum compressive residual stress at the notch tip was similar. There was more reduction in compressive residual stress in the top W coating in the 3rd case as compared to the 2nd case, as shown in Fig. 4b and c. The residual stresses in the coating lead to the bending of the coated parts. Relaxation of the residual stresses will reduce the bending of these components. A reduction in bending can be used as a parameter for comparison of the different cases here. Fig. 5a shows the deflection of these simulated coated sections vs the distance along the length of the section. Deflection was measured on the bottom side of the section. It can be seen that the maximum deflection was observed in the case of the coated section without any notch, as expected. In other cases, the deflection was reduced due to the relief of residual stresses. Coated sections with a

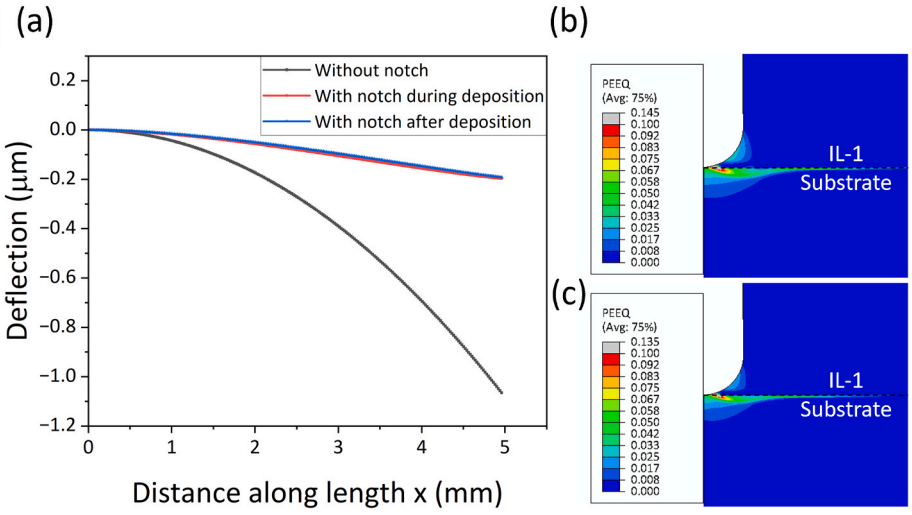

Fig. 5. a) Plot of deflection vs distance along the length for the coated section without a notch, with a notch during deposition, and with a notch after deposition. Equivalent plastic strain (PEEQ) contour at the notch tip for coated section b) with a notch during deposition c) with a notch after deposition.

notch during deposition and a notch after deposition, both have similar deflection. Based on this, it can be concluded that both strategies are effective in reducing residual stresses and recovery of bending in the coated sections. So, the strategy of castellation will be effective for large, coated components.

Apart from the advantage of stress relaxation, there was a compressive stress concentration in front of the notch tip as shown in Fig. 4b and c. Fig. 5b and c show the equivalent plastic strain at the notch tip for the coated section with notch during deposition and after deposition, respectively. It was observed that in both cases there was plastic deformation in the substrate at the notch tip which is not favorable for component stability. Since these components will be subjected to thermal cycling during operation, the plastic deformation will get higher. To gain the advantage of stress relaxation without risking the component stability, a shorter notch can be created.

3.1.2. Optimization of notch depth

It was feasible to make the notch after deposition by machining, so further simulations to find the optimized notch depth were performed using the third case model in this work. Five FEM simulations were performed with a notch after deposition with a depth of 1.16, 1.4, 1.64, 1.67 and 1.88 mm. These notch depths were chosen to position the notch tip in IL-4 to IL-1. The purpose of these simulations was to determine the notch depth that does not create plastic strain in the steel substrate. Fig. 6a shows the equivalent plastic strain vs the distance along the thickness. An undeformed model shape was used for a distance along the thickness. It was observed that the notch in interlayer (IL) 3 and 4 does not create any significant plastic strain in the steel substrate. While a notch depth of 1.67 mm in IL-2 ends the zone of significant plastic deformation just before the steel substrate. So, the notch depths less than and equal to 1.67 are considered optimized for castellation. Fig. 6b shows the deflection in the coated section for the notch of different depths. Coated section deflection was found to be increasing with decreasing notch depth. However, with the notch depth of 1.67 mm, a recovery in bending without producing any significant plastic deformation in the steel substrate is possible. So, the maximum notch depth of 1.67 mm will be suitable for large, coated plates. This optimized notch depth corresponds to nearly 70 % of the FGM layer, and it ends nearly at the middle of interlayer 2.

A notch width of 0.3 mm was considered for castellation in this work. A larger notch width corresponds to a larger notch tip radius, which increases the crack resistance of the material [38]. Rubel et al. [39] found that the deposition of deuterium and other metals increases with increasing widths of castellation from 0.5 mm to 2 mm. They recommended using the smallest width of castellation. Although the study focused on the castellation of bulk material, the trend of deuterium deposition will be the same in coatings. The minimum width studied was 0.5 mm, but no reason was mentioned for not using an even lower width. A notch width of 0.3 mm was used in this work to enhance the crack resistance and reduce deuterium deposition. Another reason for choosing 0.3 mm width was the feasibility of machining using an EDM wire with a 0.25 mm diameter, which is the most common practical size available for machining.

3.1.3. Effect of castellation during heat flux

Fig. 7a shows the coating surface temperature under a heat flux cycle with maximum heat flux of 0.25, 0.34, and 0.35 MW/m^2. A heat flux cycle with a maximum heat flux of 0.34 MW/m^2 generates a temperature close to 550 °C. Since 550 °C is the desired DEMO First Wall temperature, the heat flux cycle with maximum heat flux of 0.34 MW/m^2 was chosen for comparison between the coated section without and with notch simulations. Fig. 7b shows the plot of deflection vs distance along the length for the coated section without a notch, and with a notch at the end of the heat flux cycle with maximum heat flux of 0.34 MW/m^2.

Fig. 7c shows the thermal stress contour (S_{11}) for the coated section without and with a notch (1.67 mm) at the end of the heat flux cycle. The thermal stress in the coated section with a notch was lower than the coated section without a notch in most areas. The compressive stress in the top W coating and interlayers was also reduced due to the notch. Also, there was a reduction in tensile thermal stress in the steel substrate near the notch.

A slightly higher tensile stress in steel away from the notch was developed in the notched coated section as compared to the coated section without a notch. Also, there was a higher compressive stress in the coating below the notch than the maximum compressive stress in the coated section without a notch. The overall effect of castellation in the coated section during the heat flux cycle can be correlated using a comparison of deformation (plot of deflection), as shown in Fig. 7b. The deflection was reduced significantly for the coated section with a notch.

Based on the comparison of the coated section with and without a notch, it can be interpreted that the castellation helps in reducing residual stress and deflection after deposition (Fig. 6b) and also at the end of the heat flux cycle (Fig. 7b and c). This shows the overall advantage of castellated coatings over the without notch coatings.

3.2. Experimental results

3.2.1. Experimental validation of castellation

Experiments of castellation were performed to verify the recovery in bending of coated plates as predicted by simulations. Long beams were taken for castellation to obtain significant recovery making measurements easier. The purpose of this was to measure the recovery in deflection due to castellation as predicted by simulations in section 3.1. Fig. 8a shows one of the samples after castellation. The notch depth of

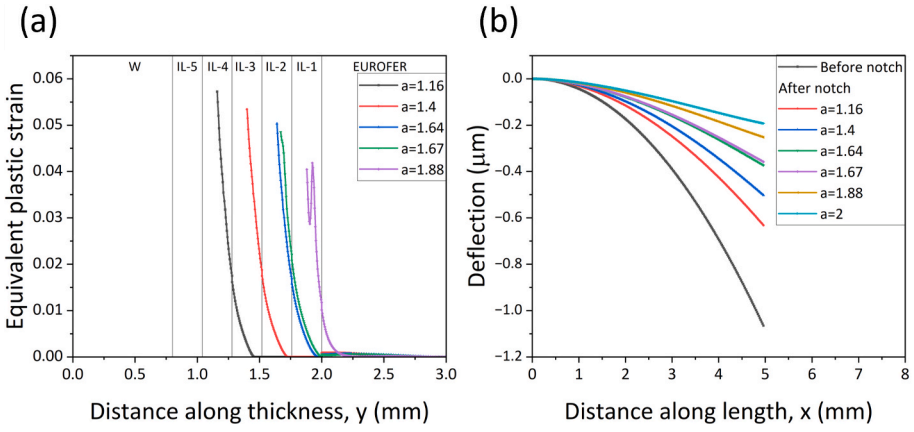

Fig. 6. a) Plot of equivalent plastic strain vs distance along the thickness for a coated section with different notch depths. b) Plot of deflection vs distance along the length of a coated section with different notch depths.

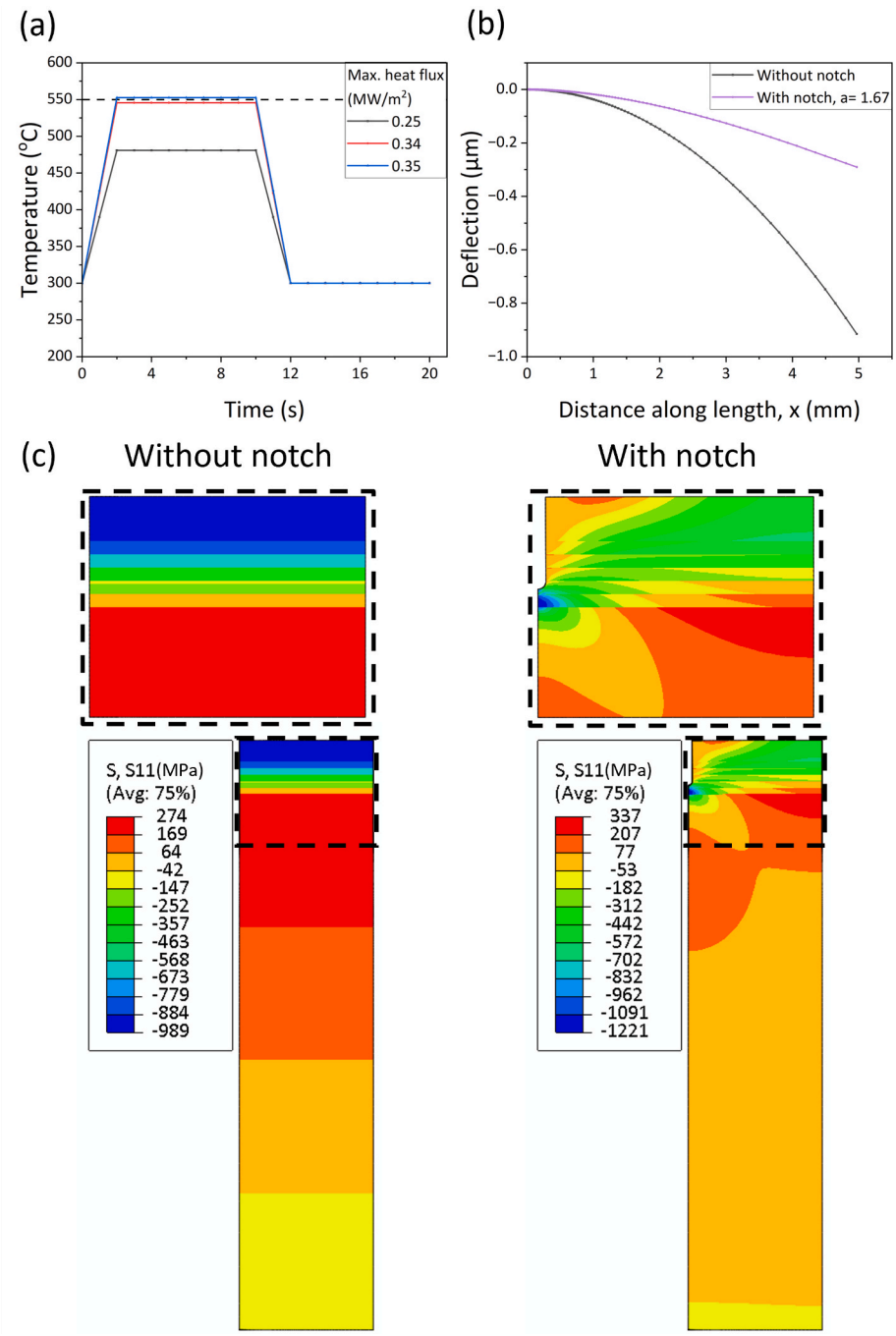

Fig. 7. a) Plot of coating surface temperature under a heat flux cycle with max. heat flux of 0.25, 0.34 and 0.35 MW/m^2, b) Plot of deflection vs distance along the length for the coated section without a notch, and with a notch at the end of the heat flux cycle with max. heat flux of 0.34 MW/m^2, and c) Thermal stress (S_{11}) contour of coated section without notch and coated section with notch at the end of heat flux cycle.

each sample was measured using an optical microscope image, and the average values are given in Table 2. The notch depth for samples S_L1, S_L2 and S_L3_1 was found close to the desired notch depth (1388 µm ± 43 µm). Sample 3(S_L3_1) was notched first up to the desired depth of 1388 µm ± 43 µm, similar to samples 1 and 2. Afterward, the notch depth of sample 3(S_L3_2) was extended to the desired notch depth of 1627 µm ± 54 µm, similar to samples 4 and 5. Fig. 8b shows the deflection of long beams before and after castellation. It can be observed that the deflection of the beam was reduced after castellation. The deflection before and after castellation was similar for all 3 samples (S_L1, S_L2 and S_L3_1) with similar notch depth, which shows the enhanced repeatability of castellation. Similarly, the other 3 samples (S_L3_2, S_L4 and S_L5) with similar notch depth also show repeatability. Some scatter in the data can be seen due to measurement error. For a better comparison, all the data were fitted with a 4-order polynomial for all cases as shown in Fig. 8b. Fitted data was plotted with a 4 mm increase in distance along the length which is similar to experimental measurements. Deflection before the notch increases from left to right of the sample with a peak nearly at the center of the sample. While the deflection of after notch sample initially increases from left to right, reaches a peak, and then decreases. A peak and valley were observed in deflection of after notch samples. To understand this peak and valley in the deflection, points A' and B' were chosen. Point A' corresponds to the maximum deflection in the fitted curve of samples before the notch. While point B' corresponds to

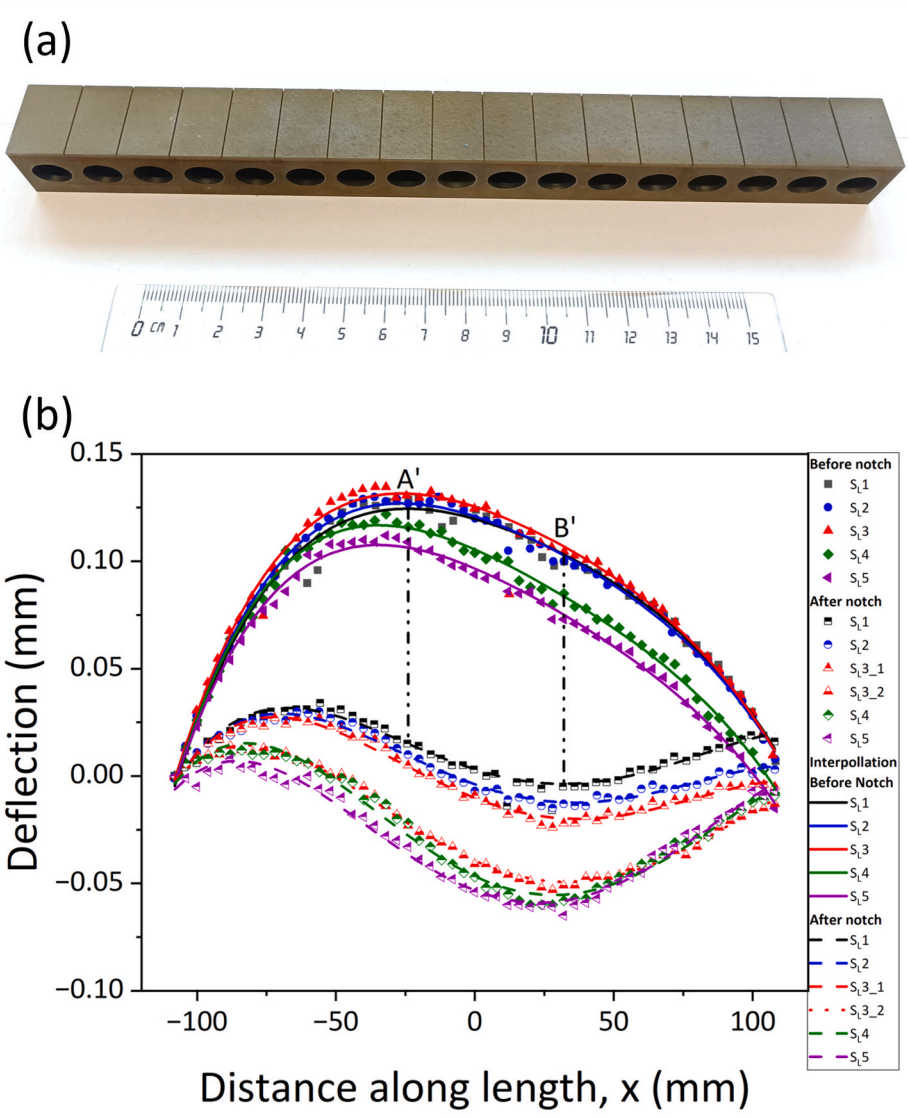

Fig. 8. a) One of the samples after castellation b) deflection of samples before and after machining the notches measured at the center of the sample.

Table 2
Details of castellation samples. Error bars of notch depth show 95 % confidence interval.

Sample	Notch depth (μm)	Position of A' (mm)	Recovery at A' (mm)	Recovery at A' (%)	Position of B' (mm)	Recovery at B' (mm)	Recovery at B' (%)
S_L1	1263 ± 21	−24	0.11	88	32	0.11	104
S_L2	1232 ± 18	−28	0.12	91	36	0.11	112
S_L3_1	1291 ± 22	−28	0.12	95	36	0.12	119
S_L3_2	1541 ± 21	−28	0.15	114	32	0.16	146
S_L4	1517 ± 14	−36	0.13	114	28	0.14	164
S_L5	1513 ± 18	−36	0.13	124	24	0.14	173

minimum deflection in the fitted curve of samples after the notch. Points A' and B' for fitted data of S_L1 are shown in Fig. 8b. The recovery in deflection due to castellation was measured at both points which is nearly the same (0.11 mm). Similarly, the recovery at A' and B' for other samples was also similar as shown in Table 2. Point A' and B' are nearly symmetric about the center. This shows that the absolute recovery in the deflection was nearly symmetric for the beam. Here, recovery greater than 100 % indicates the deflection of the beam in the other direction. Recovery of samples with maximum optimized notch depth (S_L3_2, S_L4 and S_L5) was higher than the samples S_L1, S_L2 and S_L3_1. The recovery in the deflection of the beam was increased by increasing the notch depth as predicted by simulations in section 3.1. Recovery greater than 100 % can lead to deflection of the beam in the reverse direction, which can be avoided by optimizing the number of notches. The number of notches can't be universal since it will depend on the shape and size of the First Wall. Hence, an optimization of the number of notches will be required during the application of castellation in the First Wall components.

Significant recovery was achieved in the beam by castellation. Reduction in the deflection of the beam shows the decrease of the coating's residual stresses which is beneficial for the First Wall application of these coatings. This experiment shows successful proof of principle for the castellation of coatings.

In this work, castellation of coatings was performed by EDM cutting after the deposition. A castellation of the large, coated sample was

achieved successfully, indicating the scalability of the castellation process using EDM cutting. On the other hand, performing castellation during deposition can be difficult, especially on a large scale. Machining of tungsten to create castellation was already used in ASDEX Upgrade (AUG) W tiles [23], indicating that the castellation of coatings by EDM will also be economically viable.

3.2.2. Thermal fatigue test

The developed W/EUROFER FGM coatings will be used to protect the First Wall, where they will be subjected to thermal fatigue. Due to castellation, a stress concentration will occur near the tip of the notch created, which can lead to failure. A thermal fatigue test using induction heating was performed on a small cylindrical coating sample to analyze the effect of thermal stresses on the notch. A similar induction heating-based thermal fatigue testing method was used for a cylindrical W coating sample in the literature [7]. The dimensions of the thermal fatigue sample were chosen based on the heating method used in the experiments, confirming that a uniform heating condition can be maintained [40]. Uniform heating can occur for 5 mm diameter cylindrical samples using induction heating, which was used in this work. Fig. 9 shows the SEM image of the cross-section of the coating sample subjected to 0, 500, 1000, 1500, 2000, and 5000 cycles. No crack was found in all samples after the thermal cyclic tests.

Fig. 10 shows the magnified image near the notch for the coated samples subjected to 0, 500, 1000, 1500, 2000, and 5000 cycles. It can be observed that in the case of the sample with 0 cycles, there is no negative effect of EDM machining. Zammuto et al. [23] have reported micro-cracks in W tiles due to machining. In the case of coating, no micro-cracks can be observed. No crack at the notch tip was observed till 5000 thermal cycles of the notched coated sample.

Emmerich et al. [36] performed thermal fatigue tests on a similar W/EUROFER FGM coating and reported durability of coatings for at least 5000 cycles. Based on microstructure of notched samples, no effect on the interface and substrate was found after the thermal cyclic test. This verifies that the castellated coating is stable up to at least 5000 cycles of thermal cyclic load in future fusion-relevant conditions. The same endurance of castellated coating under thermal cycles was found compared to non-castellated coatings. These notches were prepared after optimization by simulation, so there was presumably no effect of the notch on the substrate which gave the advantage during thermal cyclic test. The notch tip ends in interlayer 2 which has 37 % tungsten and 63 % of EUROFER. This makes the interlayer-2 ductile which prevents crack initiation due to the thermal stress induced in front of the notch tip. Also, stiff W splats in front of the notch tip, strengthen the material. Castellation helps in the relief of thermal stress developed during thermal cycling. All these factors resist any crack formation in the

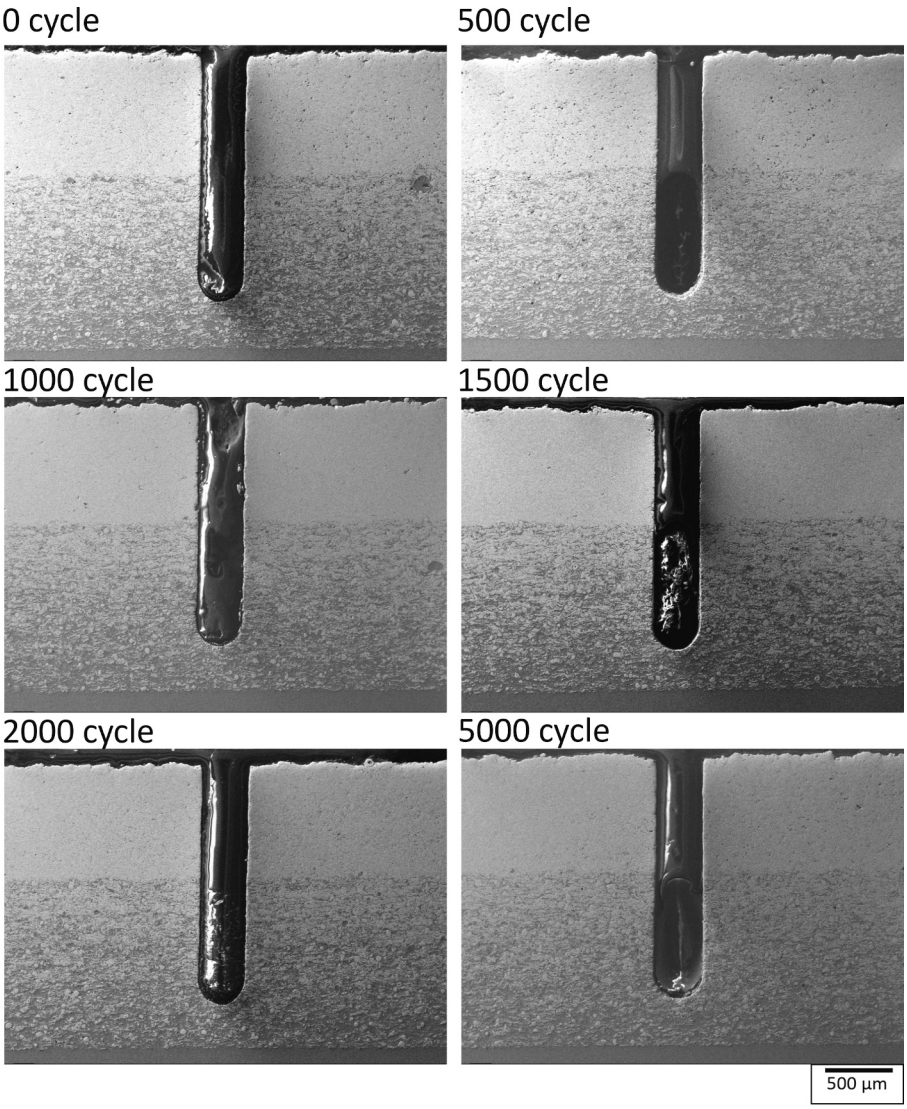

Fig. 9. SEM image of the cross-section of a notched sample after 0, 500, 1000, 1500, 2000, and 5000 thermal fatigue cycles.

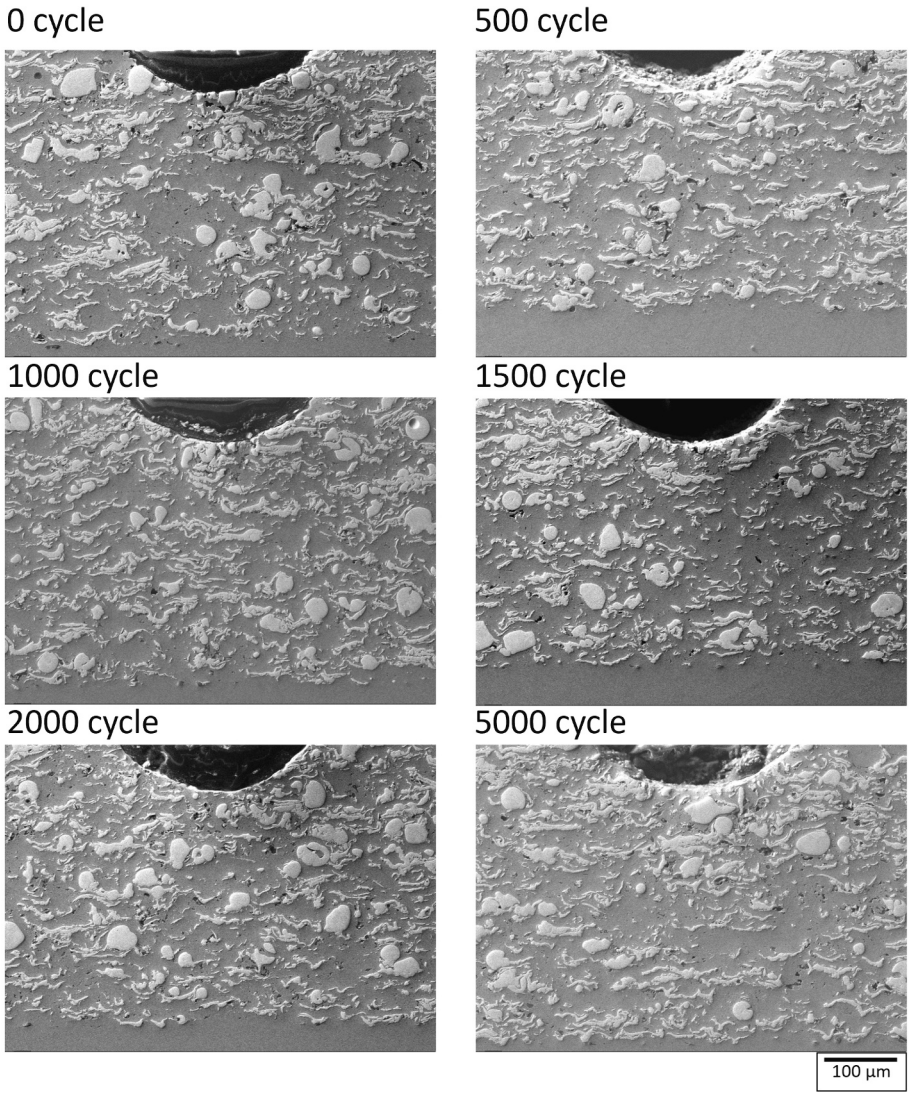

Fig. 10. Magnified SEM image of cross-section near notch after 0, 500, 1000, 1500, 2000, and 5000 thermal fatigue cycles.

coating and at the notch tip.

Castellation of coating was found to be a better way to reduce thermal stress in coatings as compared to other stress relief methods, such as micro-engineered textured tungsten coating [22] and vertically crack W coatings [7]. Micro-engineered coatings [22] were developed by the CVD method on micron-scale, which have not yet been explored for thicker coatings required for the DEMO First Wall application. In the case of vertically crack coating [7], the crack tip was sharp, which decreases the crack resistance properties of the coating, leading to early failure. Also, it's not possible to precisely control the position and depth of vertical cracks. Castellation can be performed more precisely by making a notch using an EDM method, and its implementation is shown effectively on a large scale in this work.

4. Conclusion and outlook

This work presents a novel approach of the castellation of W/EUROFER FGM coatings using finite element simulations and experimental validation. The main conclusions are the following:

1. Finite element simulations were performed for coatings deposited without castellation, with castellation during deposition and castellation after deposition. The advantage of castellation was a reduction in residual stresses and bending of components. However, it showed plastic deformation at the notch tip in the substrate.
2. An optimized notch depth was determined by finite element simulation of castellation after deposition, to gain the advantage of castellation without deforming the substrate. A notch until nearly half of interlayer 2 (37 % tungsten and 63 % of EUROFER) was found to be best suited for castellation.
3. Finite element simulations show that the deformation for the castellated coated section was lower than the coated section without a notch under the DEMO First Wall relevant heat flux cycle.
4. Castellation was performed on coated samples and their deflection was measured before and after machining the notch. After the castellation, a reduction in the deflection of the beam-shaped samples was found which also indicates a reduction in the residual stresses. A good reproducibility was obtained for all samples. This proves the principle of castellation in the coating.
5. Thermal fatigue tests with fusion-relevant temperature conditions were performed on castellated coating samples, and the notched samples remained stable and crack-free till at least 5000 cycles.

In the current work, a small, coated section was simulated to find the optimal notch depth. A large, coated component can be simulated in the future to optimize the number of notches required. Also, that should be

based on a specific dimension of the First Wall of a fusion reactor. The effect of notch width on deuterium deposition and fracture properties of coatings can be determined experimentally.

CRediT authorship contribution statement

Ashwini Kumar Mishra: Writing – review & editing, Writing – original draft, Visualization, Validation, Software, Methodology, Investigation, Formal analysis, Conceptualization. **Thilo Grammes:** Writing – review & editing, Methodology, Conceptualization. **Jarir Aktaa:** Writing – review & editing, Supervision, Funding acquisition, Conceptualization.

Declaration of competing interest

The authors declare that they have no known competing financial interests or personal relationships that could have appeared to influence the work reported in this paper.

Acknowledgments

The authors would like to thank Mr. Daniel Kuntz and Ms. Ute Gretz from TEC, KIT, Germany, for sample preparation and measuring deflection using a 3D coordinate measuring machine. The authors would like to thank Ms. Melina Blem (IAM, KIT, Germany) for her help in sample preparation and Dr. Thomas Emmerich (formerly IAM, KIT, Germany) for his help with the thermal fatigue test apparatus.

This work has been carried out within the framework of the EUROfusion Consortium, funded by the European Union via the Euratom Research and Training Programme (Grant Agreement No 101052200 — EUROfusion). Views and opinions expressed are however those of the author(s) only and do not necessarily reflect those of the European Union or the European Commission. Neither the European Union nor the European Commission can be held responsible for them.

Data availability

Data will be made available on request.

References

[1] X. Yang, W. Qiu, L. Chen, J. Tang, Tungsten–potassium: a promising plasma-facing material, Tungsten 1 (2019) 141–158, https://doi.org/10.1007/s42864-019-00018-5.

[2] C. Luo, L. Xu, L. Zong, H. Shen, S. Wei, Research status of tungsten-based plasma-facing materials: a review, Fusion Eng. Des. 190 (2023) 113487, https://doi.org/10.1016/j.fusengdes.2023.113487.

[3] J. Matějíček, B. Nevrlá, M. Vilémová, H. Boldyryeva, Overview of processing technologies for tungsten-steel composites and FGMs for fusion applications, Nukleonika 60 (2015) 267–273, https://doi.org/10.1515/nuka-2015-0049.

[4] R. Vaßen, K.-H. Rauwald, O. Guillon, J. Aktaa, T. Weber, H.C. Back, D. Qu, J. Gibmeier, Vacuum plasma spraying of functionally graded tungsten/EUROFER97 coatings for fusion applications, Fusion Eng. Des. 133 (2018) 148–156, https://doi.org/10.1016/j.fusengdes.2018.06.006.

[5] D.D. Qu, W.W. Basuki, J. Gibmeier, R. Vaßen, J. Aktaa, Development of functionally graded tungsten/EUROFER coating system for first wall application, Fusion Sci. Technol. 68 (2015) 578–581. https://doi.org/10.13182/FST15-113.

[6] T. Grammes, T. Emmerich, J. Aktaa, W/EUROFER functionally graded coatings for plasma facing components: technology transfer to industry and upscaling, Fusion Eng. Des. 173 (2021) 112940, https://doi.org/10.1016/j.fusengdes.2021.112940.

[7] W. Cui, K. Flinders, D. Hancock, P.S. Grant, Joining and cycling performance of ultra-thick tungsten coatings on patterned steel substrates for fusion armour applications, Mater. Des. 212 (2021) 110250, https://doi.org/10.1016/j.matdes.2021.110250.

[8] R. Neu, H. Maier, B. Böswirth, S. Elgeti, H. Greuner, K. Hunger, J. Kondas, A. von Müller, Investigations on cold spray tungsten/tantalum coatings for plasma facing applications, Nucl. Mater. Energy 34 (2023) 101343, https://doi.org/10.1016/j.nme.2022.101343.

[9] J. Matějíček, R. Dejarnac, C. Ruset, E. Grigore, L. Cvrček, J. Walter, F. Perry, Development of tungsten coatings on Inconel superalloy for COMPASS upgrade plasma-facing components, Nucl. Mater. Energy 42 (2025) 101844, https://doi.org/10.1016/j.nme.2024.101844.

[10] Z. Chen, Y.-Y. Lian, X. Liu, F. Feng, B.-Y. Yan, J.-B. Wang, Y.-W. Lv, J.-P. Song, C.-J. Liu, L.-Z. Cai, Recent research and development of thick CVD tungsten coatings for fusion application, Tungsten 2 (2020) 83–93, https://doi.org/10.1007/s42864-020-00041-x.

[11] J.W. Coenen, V.Y.S. Lee, Y. Mao, A. Morrison, D. Dorow-Gerspach, X. Tan, A. Terra, Y. Wu, C. Linsmeier, Evolution of tungsten fiber-reinforced tungsten-remarks on production and joining, Adv. Eng. Mater. 25 (2023), https://doi.org/10.1002/adem.202300569.

[12] T. Weber, J. Aktaa, Numerical assessment of functionally graded tungsten/steel joints for divertor applications, Fusion Eng. Des. 86 (2011) 220–226, https://doi.org/10.1016/j.fusengdes.2010.12.084.

[13] D.D. Qu, W.W. Basuki, J. Aktaa, Numerical assessment of functionally graded tungsten/EUROFER coating system for first wall applications, Fusion Eng. Des. 98–99 (2015) 1389–1393, https://doi.org/10.1016/j.fusengdes.2015.06.120.

[14] T. Emmerich, D. Qu, B.-E. Ghidersa, M. Lux, J. Rey, R. Vaßen, J. Aktaa, Development progress of coating first wall components with functionally graded W/EUROFER layers on laboratory scale, Nucl. Fusion 60 (2020) 126004, https://doi.org/10.1088/1741-4326/aba336.

[15] T. Grammes, T. Emmerich, D. Qu, O. Heinze, R. Vaßen, J. Aktaa, Functionally graded tungsten/EUROFER coating for DEMO first wall: from laboratory to industrial production, Fusion Eng. Des. 188 (2023) 113430, https://doi.org/10.1016/j.fusengdes.2023.113430.

[16] T. Grammes, A.K. Mishra, K. Battalov, A. Purwitasari, T. Emmerich, J. Aktaa, Mechanical properties and quality of plasma sprayed, functionally graded tungsten/steel coatings after process upscaling, Mater. Chem. Phys. 311 (2024) 128530, https://doi.org/10.1016/j.matchemphys.2023.128530.

[17] P.Y. Piskarev, A.A. Gervash, D.A. Glazunov, E.V. Okuneva, I.V. Mazul, A. V. Krasilnikov, A.B. Putrik, V.E. Kuznetsov, R.V. Rulev, V.V. Ruzanov, A. Y. Ogursky, S.V. Bobrov, A.V. Lapin, T.M. Gurieva, D.V. Lyanzberg, M. A. Panteleev, I.V. Sokolov, N.A. Makhankov, V.A. Vasiliev, V.V. Levichev, High heat flux components with beryllium armour: from the small-scale mock-ups to the full-scale prototype of the ITER first wall panel, Fusion Eng. Des. 203 (2024) 114473, https://doi.org/10.1016/j.fusengdes.2024.114473.

[18] G.-N. Luo, G.H. Liu, Q. Li, S.G. Qin, W.J. Wang, Y.L. Shi, C.Y. Xie, Z.M. Chen, M. Missirlian, D. Guilhem, M. Richou, T. Hirai, F. Escourbiac, D.M. Yao, J.L. Chen, T.J. Wang, J. Bucalossi, M. Merola, J.G. Li, EAST Team, Overview of decade-long development of plasma-facing components at ASIPP, Nucl. Fusion 57 (2017) 065001, https://doi.org/10.1088/1741-4326/aa6502.

[19] Q. Li, P. Qi, H.S. Zhou, Y.Y. Zhang, Z.S. Yang, J. Wu, G.-N. Luo, J.G. Li, PFM Group, R&D issues of W/Cu divertor for EAST, Fusion Eng. Des. 85 (2010) 1106–1112, https://doi.org/10.1016/j.fusengdes.2010.02.017.

[20] Y. Xu, C.Y. Xie, S.G. Qin, J.P. Song, Q. Li, S.X. Zhao, G.H. Liu, T.J. Wang, Y. Yu, G.-N. Luo, Preliminary R&D on flat-type W/Cu plasma-facing materials and components for Experimental Advanced Superconducting Tokamak, Phys. Scr. T159 (2014) 014008, https://doi.org/10.1088/0031-8949/2014/T159/014008.

[21] I. Bobin Vastra, B. Schedler, M. Merola, F. Jacquinot, A. Cottin, D. Cauvin, M. Febvre, Y. Leblanc, Manufacturing of prototype components for the ITER divertor baffle, Fusion Eng. Design 66–68 (2003) 341–346. https://doi.org/10.1016/S0920-3796(03)00389-2.

[22] S. Sharafat, A. Aoyama, B. Williams, N. Ghoniem, Development of micro-engineered textured tungsten surfaces for high heat flux applications, J. Nucl. Mater. 442 (2013) S302–S308, https://doi.org/10.1016/j.jnucmat.2013.05.004.

[23] I. Zammuto, A. Herrmann, N. Jaksic, M. Li, M. Balden, V. Rohde, S. Vorbrugg, H. Greuner, R. Neu, A. Kallenbach, the ASDEX Upgrade Team, Measures to overcome deep cracks of tungsten tiles in the ASDEX upgrade divertor, Fusion Eng. Des. 146 (2019) 2434–2437, https://doi.org/10.1016/j.fusengdes.2019.04.011.

[24] G. Zhou, F.A. Hernández, P. Pereslavtsev, B. Kiss, A. Retheesh, L. Maqueda, J. H. Park, The European DEMO helium cooled pebble bed breeding blanket: design status at the conclusion of the pre-concept design phase, Energies 16 (2023) 5377, https://doi.org/10.3390/en16145377.

[25] E. Gaganidze, Material Property Handbook Tungsten, EUROfusion Internal Document IDM2P3SPL, 2020.

[26] F. Tavassoli, Fusion Demo Interim Structural Design Criteria (DISDC) - Appendix A Material Design Limit Data - A3.S18E Eurofer Steel, CEA DEN-SAC DMN Technical Report DMN/DIR/NT/2004-02/A, 2004.

[27] E. Gaganidze, Material Property Handbook EUROFER97, EUROfusion Internal Document IDM2NZHBS, 2022.

[28] X.C. Zhang, B.S. Xu, H.D. Wang, Y.X. Wu, Y. Jiang, Effects of compositional gradient and thickness of coating on the residual stresses within the graded coating, Mater. Des. 28 (2007) 1192–1197, https://doi.org/10.1016/j.matdes.2006.01.012.

[29] S. Adachi, GaAs, AlAs, and Al x Ga1− x As: Material parameters for use in research and device applications, J. Appl. Phys. 58 (1985) R1–R29, https://doi.org/10.1063/1.336070.

[30] G. Thomas, R. Vincent, G. Matthews, B. Dance, P.S. Grant, Interface topography and residual stress distributions in W coatings for fusion armour applications, Mater. Sci. Eng. A 477 (2008) 35–42, https://doi.org/10.1016/j.msea.2007.05.120.

[31] T. Nagasaka, R. Kasada, A. Kimura, Y. Ueda, T. Muroga, Theromophysical properties and microstructure of plasma-sprayed tungsten coating on low activation materials, Fusion Sci. Technol. 56 (2009) 1053–1057, https://doi.org/10.13182/FST56-1053.

[32] B. Chelihi, C. Garnier, J. Aubert, G. Zhou, Dedicated thermo-mechanical analyses in support of DEMO HCPB BB design, Fusion Eng. Des. 213 (2025) 114872, https://doi.org/10.1016/j.fusengdes.2025.114872.

[33] P.J. Ennis, A. Zielinska-Lipiec, O. Wachter, A. Czyrska-Filemonowicz, Microstructural stability and creep rupture strength of the martensitic steel P92 for advanced power plant, Acta Mater. 45 (1997) 4901–4907, https://doi.org/10.1016/S1359-6454(97)00176-6.
[34] K. Mergia, N. Boukos, Structural, thermal, electrical and magnetic properties of Eurofer 97 steel, J. Nucl. Mater. 373 (2008) 1–8, https://doi.org/10.1016/j.jnucmat.2007.03.267.
[35] I. Zammuto, L. Giannone, A. Herrmann, A. Houben, A. Kallenbach, K. H. Schuhbeck, B. Sieglin, S. Vorbrugg, the ASDEX Upgrade Team, Implementation of ferritic steel as in vessel wall: Lessons learnt and follow up, Fusion Eng. Des. 124 (2017) 297–301, https://doi.org/10.1016/j.fusengdes.2017.04.016.
[36] T. Emmerich, R. Vaßen, J. Aktaa, Thermal fatigue behavior of functionally graded W/EUROFER-layer systems using a new test apparatus, Fusion Eng. Des. 154 (2020) 111550, https://doi.org/10.1016/j.fusengdes.2020.111550.
[37] H. Bolt, V. Barabash, G. Federici, J. Linke, A. Loarte, J. Roth, K. Sato, Plasma facing and high heat flux materials – needs for ITER and beyond, J. Nucl. Mater. 307–311 (2002) 43–52, https://doi.org/10.1016/S0022-3115(02)01175-3.
[38] S. Cicero, V. Madrazo, I.A. Carrascal, Analysis of notch effect in PMMA using the theory of critical distances, Eng. Fract. Mech. 86 (2012) 56–72, https://doi.org/10.1016/j.engfracmech.2012.02.015.
[39] M. Rubel, P. Petersson, Y. Zhou, J.P. Coad, C. Lungu, I. Jepu, C. Porosnicu, D. Matveev, A. Kirschner, S. Brezinsek, A. Widdowson, E. Alves, Fuel inventory and deposition in castellated structures in JET-ILW, Nucl. Fusion 57 (2017) 066027, https://doi.org/10.1088/1741-4326/aa6864.
[40] F. Schoofs, M. Gorley, A route to standardised high heat flux testing: an example for tungsten, Fusion Eng. Des. 139 (2019) 132–136, https://doi.org/10.1016/j.fusengdes.2018.12.060.